considering the Lagrangian derivative of pressure on an isentropic surface:

$$\frac{dp}{dt} = \omega = \frac{\partial p}{\partial t} + u \frac{\partial p}{\partial x} + v \frac{\partial p}{\partial y} + \frac{d\theta}{dt} \left(\frac{\partial p}{\partial \theta} \right)$$
(4.25)

where all the derivatives are taken on an isentropic surface. Under adiabatic conditions, the last term on the RHS of (4.25) can be neglected. We find, however, that an additional assumption needs to be made in order that pressure advection (the middle two terms on the RHS of (4.25)) alone can determine the sign of the vertical motion – that is, the pressure distribution has to be in steady state (i.e. $\partial p/\partial t = 0$). This condition is not often met in the atmosphere as the structure of an individual weather system is continually changing and, therefore, so is the topography of its numerous isentropic surfaces. Despite this difficulty, it is often possible to determine the sign of the vertical motion correctly by considering the pressure advection on an isentropic surface.

Finally, consider the 700 hPa isobar on the 305 K is entropic surface depicted in Figure 4.5. The Poisson equation involves temperature, pressure, and θ . Thus, there is a unique value of temperature at 700 hPa that corresponds to 305 K (namely, 275.4 K). Thus, the 700 hPa isobar on the 305 K is entropic surface corresponds exactly to the 275.4 K isotherm on the 700 hPa isobaric surface! This simple example leads us to a simple rule:

> An isobar on an isentropic surface is equivalent to an isotherm on an isobaric surface.

Thus, the diagnostic of pressure advection on an isentropic surface is very similar to that of temperature advection on an isobaric surface. As a consequence, it is not unusual for synoptic meteorologists to give a rough diagnosis of the vertical motion in a mid-latitude weather system by considering the sign of the temperature advection. This diagnostic is limited in precisely the same way as the pressure advection diagnostic we just considered with respect to Figure 4.5. It is only valid for adiabatic, steady-state conditions in which the static stability is positive. This last characteristic of the adiabatic method for diagnosing vertical motions in the isobaric coordinate system is buried in the monotonic assumption that underlies the use of isentropic coordinates. We will see in later chapters that much more satisfying diagnostics of the vertical motion in mid-latitude weather systems arise from more stringent dynamical considerations.

4.3 The Thermal Wind Balance

Recall that the hypsometric equation (3.6) suggested that the thickness between two isobaric surfaces is smaller in a cold column of air than in a warm column. Consider a hypothetical example in which a cold column and a warm column are horizontally juxtaposed, as in Figure 4.6. The distance between the 1000 and 800 hPa surfaces must be larger in the warm air than the cold so that the 800 hPa surface slopes downward

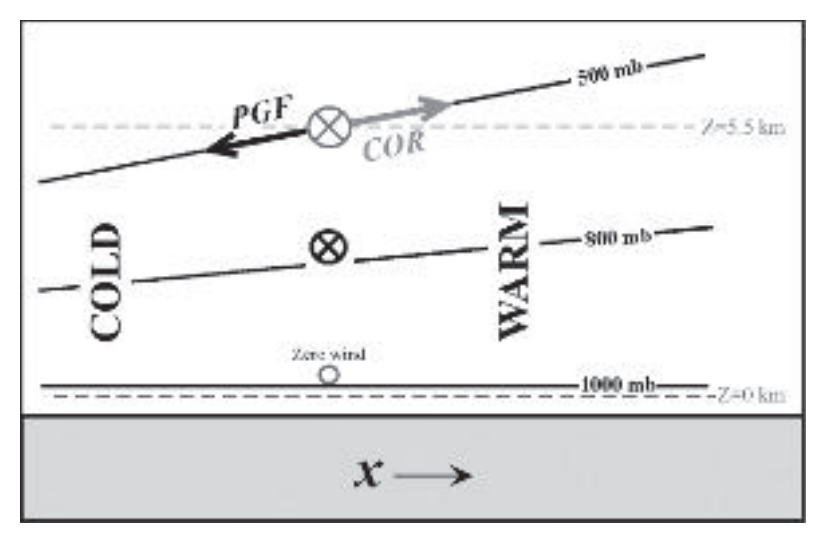


Figure 4.6 Vertical cross-section across a region of horizontal temperature contrast. Solid black lines are isobars. Dashed gray lines are elevation contours. The lack of PGF at $Z=0\,\mathrm{km}$ leads to 'Zero wind' there. At 5.5 km in the same vertical column there is a large geostrophic wind into the page, signified by the gray 'X' in the circle. The vertical shear of the geostrophic wind is signified by the darker 'X' in the center of the column

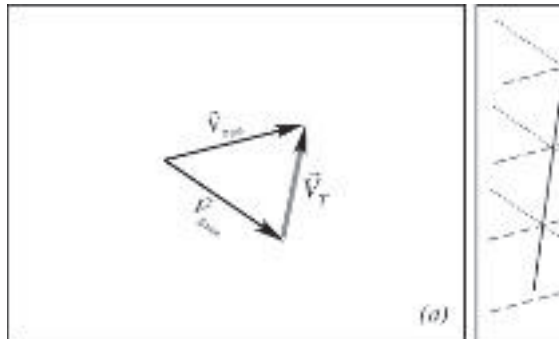
toward the cold air as illustrated. Similarly, the distance between the 800 and 500 hPa surfaces must be larger in the warm air than the cold and so the 500 hPa surface slopes even more dramatically downward toward the cold air. Thus, we find that the slope of the isobaric surfaces increases with increasing height in the presence of a horizontal contrast in column average temperature. Of course, the slope of an isobaric surface is equivalent to the existence of a geopotential gradient along that surface since the geopotential difference is simply $g\Delta z$. We now know that the pressure gradient force on an isobaric surface is related to the geopotential gradient on that surface. Thus, the increased slope to the isobaric surfaces in Figure 4.6 also means that the magnitude of the horizontal pressure gradient force increases with increasing height. Consequently, the geostrophic wind must be increasing with increasing height as well. Therefore, there is a physical relationship between the vertical shear of the geostrophic wind (i.e. the manner in which the geostrophic wind changes with height) and the horizontal temperature gradient. We now explore the mathematical description of this relationship by first considering the hydrostatic equation in isobaric coordinates.

Recall that the hydrostatic equation is given by $\partial p/\partial z = -\rho g$. This is easily rearranged into

$$\frac{g\partial z}{\partial p} = -\frac{1}{\rho} = -\frac{RT}{p} \tag{4.26a}$$

and, since $g\partial z = \partial \phi$, it can be expressed as

$$\frac{\partial \phi}{\partial p} = -\frac{RT}{p},\tag{4.26b}$$



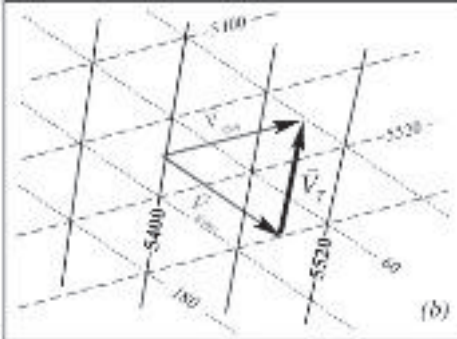


Figure 4.7 (a) Graphical depiction of the thermal wind vector obtained by subtracting the 1000 hPa geostrophic wind from the 500 hPa geostrophic wind. (b) Illustration of the relationship between the thermal wind vector and the 1000–500 hPa thickness isopleths. Dashed lines are 500 hPa geopotential heights, dotted lines are 1000 hPa geopotential heights, and the solid black lines are of 1000–500 hPa thickness. All isopleths are labeled in m and contoured every 60 m

the isobaric form of the hydrostatic equation. Now, the vertical derivative (in isobaric coordinates) of the geostrophic wind relationship $(\vec{V}_g = (\hat{k}/f) \times \nabla \phi)$ is

$$\frac{\partial \vec{V}_g}{\partial p} = \frac{\hat{k}}{f} \times \nabla \frac{\partial \phi}{\partial p}.$$
 (4.27a)

Substituting for $\partial \phi / \partial p$ from (4.26b) yields

$$\frac{\partial \vec{V}_g}{\partial p} = \frac{\hat{k}}{f} \times \nabla - \frac{RT}{p} = \left(\frac{-R}{fp}\right) \hat{k} \times \nabla T \tag{4.27b}$$

confirming the physics depicted in Figure 4.6: that the vertical shear of the geostrophic wind is directly related to the horizontal temperature gradient. Based upon this temperature gradient dependence, the vertical shear of the geostrophic wind is known as the **thermal wind**. The component form of (4.27b) yields

$$\frac{\partial u_g}{\partial p} = \frac{R}{fp} \frac{\partial T}{\partial y}$$
 and $\frac{\partial v_g}{\partial p} = -\frac{R}{fp} \frac{\partial T}{\partial x}$. (4.28)

Returning to Figure 4.6, we find that $\partial T/\partial x > 0$ and therefore $\partial v_g/\partial p < 0$ which is consistent with an increase in v_g with height as depicted. In graphical form, the thermal wind vector is simply the vector difference between the geostrophic wind at some upper level in the atmosphere and the geostrophic wind at some lower level, as shown in Figure 4.7(a). Consequently, the thermal wind vector (\vec{V}_T) is actually best represented by $\vec{V}_T = -\partial \vec{V}_g/\partial p$. From (4.27a) it is clear that the thermal wind vector will be parallel to isopleths of thickness, with lower thickness to its left (right) in the northern (southern) hemisphere (Figure 4.7b). Given this physical relationship, it is possible to determine the sign of the column-averaged geostrophic temperature advection simply by knowing the direction of the thermal wind.

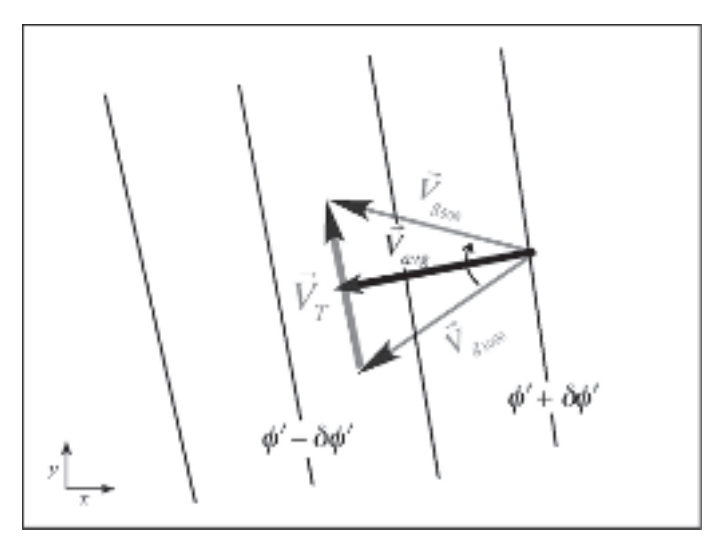


Figure 4.8 Depiction of geostrophic winds veering with height in the northern hemisphere. The thick black arrow is the column-averaged geostrophic wind. Solid lines are isopleths of 1000-500 hPa thickness. The column-averaged wind is clearly directed across thickness isopleths from large values to low values, indicative of column-averaged geostrophic warm air advection

Consider, for instance, the situation depicted in Figure 4.8 in which the geostrophic wind direction veers (turns clockwise) with height. The thermal wind vector, as represented by the thick arrow, is given by $\vec{V}_T = \vec{V}_{g_{500}} - \vec{V}_{g_{1000}}$. Assuming the situation is occurring in the northern hemisphere, the thickness isopleths must be drawn as in Figure 4.8. The column-averaged geostrophic temperature advection is given by

$$-\overline{\vec{V}}_g \cdot \nabla \overline{T}$$
 or $-\overline{\vec{V}}_g \cdot \nabla \left(-\frac{\partial \phi}{\partial p}\right)$ (4.29)

where $\overline{\vec{V}}_g$ is the column-averaged geostrophic wind $(\overline{\vec{V}}_g = (\vec{V}_{g_{500}} + \vec{V}_{g_{1000}})/2)$ and the column-averaged temperature is related to the thickness by the hypsometric equation. Thus, we find that under these circumstances the average geostrophic wind is directed across the thickness isopleths from higher values to lower values, indicating column-averaged geostrophic warm air advection. Therefore, simple knowledge of the vertical distribution of the geostrophic wind at a point can be used to determine a portion of the temperature tendency in the vicinity of that point.

Another clear application of the thermal wind relationship that has a bearing on the structure and behavior of mid-latitude weather systems is consideration of the mid-latitude jet stream. The jet stream is a core of high-speed winds located at the top of the troposphere as shown in Figure 4.9(a). Given that the winds are predominantly geostrophic at middle latitudes, a large fraction of the total wind in the jet is described by the geostrophic wind. A vertical cross-section of geostrophic winds through the mid-latitude jet stream is shown in Figure 4.9(b). Note that there is considerable vertical shear of the geostrophic wind from ~700 to 350 hPa. The thermal wind relationship demands that this vertical shear be accompanied

by a horizontal temperature contrast. Figure 4.9(b), which also shows the vertical cross-section of potential temperature through the jet stream core, illustrates that a significant horizontal temperature contrast is present through the entire troposphere and lower stratosphere. Such a temperature contrast is characteristic of the fronts within extratropical cyclones. Figure 4.9(a) shows where the jet stream is located in relation to an associated extratropical cyclone. Notice that the jet streak, the local portion of the broader jet stream, is in the vicinity of the surface cold front. This is, of course, not an accident but a mandate since the large vertical geostrophic shears associated with the jet streak must be associated with a large horizontal temperature contrast such as the one that characterizes the cold frontal zone. This is one reason that the position of the jet stream is so important in the discussion of mid-latitude weather systems.

From a broader perspective, the thermal wind relationship also has important dynamical consequences for the general circulation of the atmosphere. Given that the Earth is an oblate spheroid, it is not heated evenly by the Sun: the equatorial regions are warmer than the polar regions. As a consequence, there is a pole to equator temperature contrast in both hemispheres so that time-averaged thickness isopleths ring the Earth like latitude lines with a poleward-directed temperature gradient vector. The thermal wind relationship mandates that this thermal contrast be reflected by the presence of *westerly vertical shear* in both hemispheres. Thus, the fundamental fact that mid-latitude weather systems move from west to east on Earth is a direct consequence of the uneven heating of the Earth by the Sun combined with the primacy of the thermal wind balance at middle latitudes.

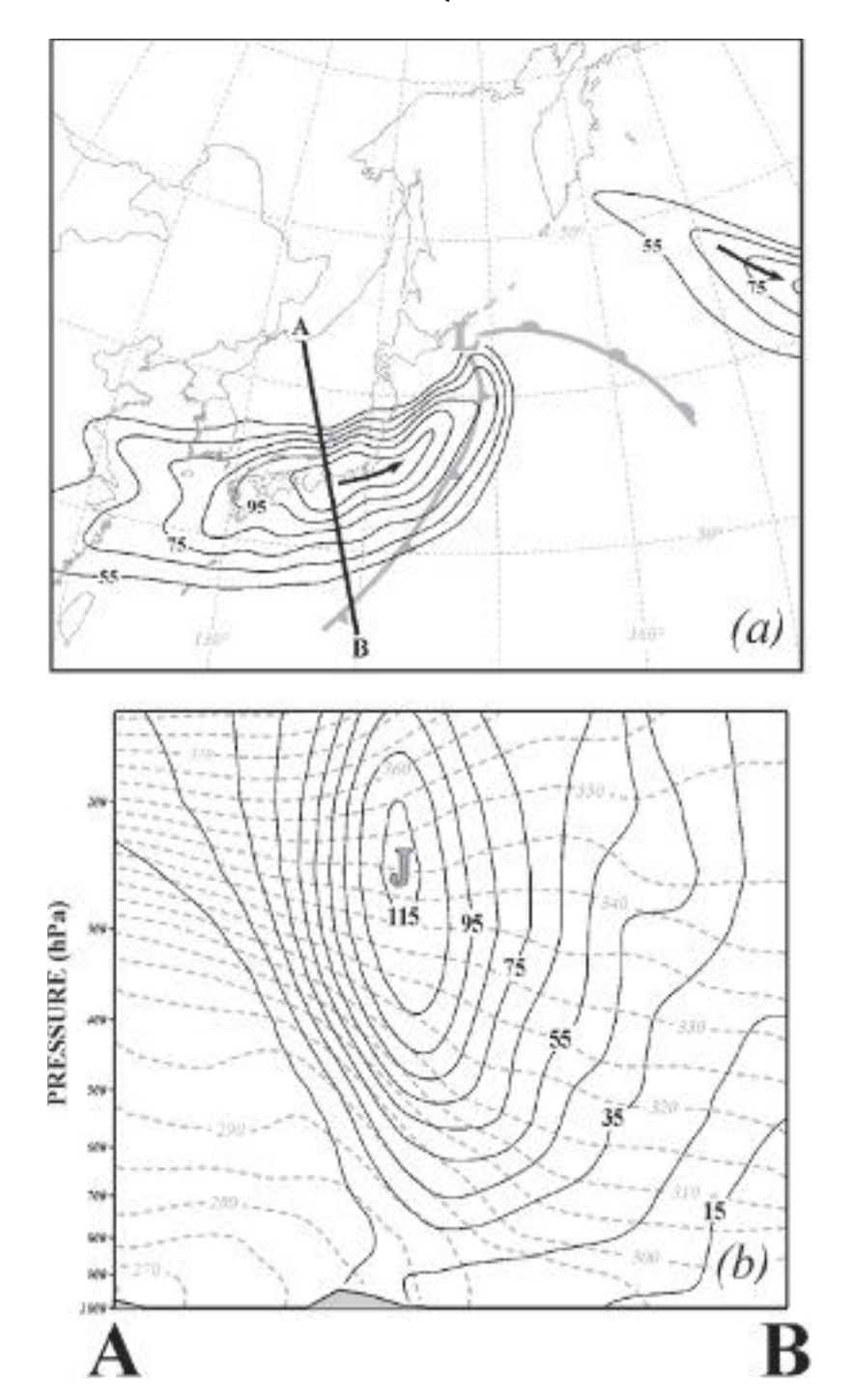
Finally, the thermal wind relationship forms the cornerstone of modern dynamical meteorology as well as the first-order balance for the flow in the middle latitudes on Earth. This latter point is a direct consequence of the fact that the mid-latitude atmosphere is, to first order, geostrophically and hydrostatically balanced. The combination of these balances into the thermal wind balance will provide us with a powerful diagnostic tool for understanding the structure, dynamics, and evolution of mid-latitude weather systems in subsequent chapters.

4.4 Natural Coordinates and Balanced Flows

It is probably clear by this point in our investigation of dynamics that, despite the potential for great complication, the gross behavior of the mid-latitude atmosphere can be understood in terms of relatively simple approximate force balances. Additional insight into the variety of simple force balances relevant to understanding the atmosphere can be achieved by idealizing the flow as steady state and purely horizontal (i.e. without vertical motions). Despite the unrealistic nature of these idealizations, important new insights arise through entertaining these simplifications.

In this section, we will again consider the frictionless equation of motion

$$\frac{d\vec{V}}{dt} = -\nabla_p \phi - f\hat{k} \times \vec{V} \tag{4.30}$$



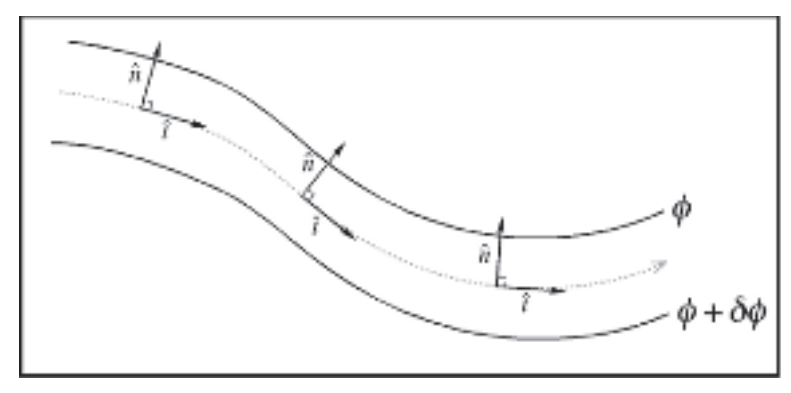


Figure 4.10 Schematic illustrating the relationship between the horizontal flow and the natural coordinate unit vectors, \hat{t} and \hat{n} . The gray dotted line is a streamline in flow parallel to geopotential height contours

but in a Cartesian coordinate system based upon the orientation of the fluid flow. Such a system is known as **natural coordinates** and it will prove to be very useful in these investigations. One might wonder why should we bother with yet another coordinate transformation? The motivation for the adoption of natural coordinates lies in the advantage it produces in describing the acceleration term in (4.30). Acceleration is a vector quantity so it can be the result of (1) a change in flow *speed*, or (2) a change in flow *direction*, resulting from curvature in the flow. Upon expanding (4.30) in a system of natural coordinates, these aspects of acceleration can be considered separately, thus providing considerable physical insight.

We begin the transformation by defining the natural coordinate system as a Cartesian coordinate system based upon a set of orthogonal unit vectors \hat{t} , \hat{n} , and \hat{k} . As illustrated in Figure 4.10, \hat{t} is oriented parallel to the horizontal velocity vector at each point, \hat{n} is oriented normal to the horizontal flow at each point such that it is positive to the left of the flow direction, and \hat{k} is directed upward. In this natural coordinate system the velocity vector, \vec{V} , is written as $\vec{V} = V\hat{t}$ where V is the magnitude of the velocity vector and can be expressed as V = ds/dt where s is a measure of the distance in the \hat{t} direction. The acceleration, $d\vec{V}/dt$, is therefore given by

$$\frac{d\vec{V}}{dt} = \frac{d}{dt}(V\hat{t}) = \hat{t}\frac{dV}{dt} + V\frac{d\hat{t}}{dt}.$$
 (4.31)

We next need to develop an expression for the rate of change of direction, $d\hat{t}/dt$. This direction change is dependent on the presence of flow curvature as illustrated

Figure 4.9 (a) The 300 hPa isotachs of the geostrophic wind at 0000 UTC 23 February 2004. Isotachs are labeled in m s $^{-1}$ and contoured every $10 \, \text{m s}^{-1}$ beginning at $55 \, \text{m s}^{-1}$. Heavy arrows indicate the direction of the wind. Vertical cross-section along line A–B shown in (b). Light gray L and frontal symbols indicate position of surface cyclone at this time. (b) Vertical cross-section of geostrophic isotachs and potential temperature along line A–B in (a). Isotachs are solid black lines labeled and contoured as in (a). Gray dashed lines are isentropes labeled in K and contoured every 5 K. Note that the region of maximum vertical shear is also the region of maximum horizontal temperature gradient throughout the troposphere

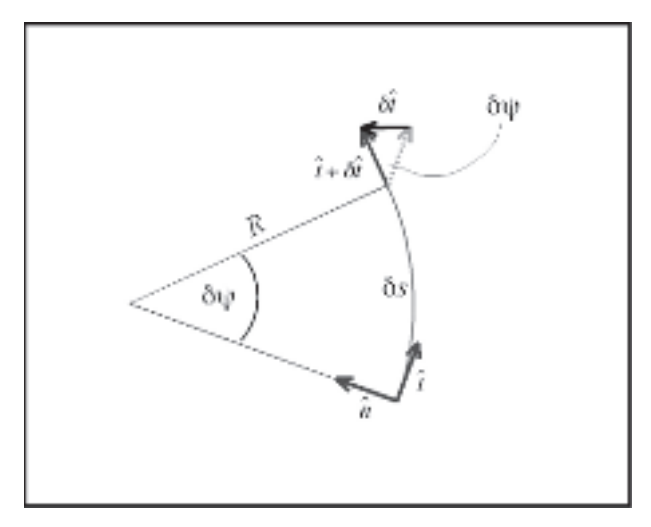


Figure 4.11 The rate of change of the natural coordinate vector \hat{t} following the motion. R is the radius of curvature of the parcel trajectory

in Figure 4.11. In order to describe this curvature, we adopt the convention that the radius of curvature of parcel trajectories (i.e. R= radius of curvature *following the parcel motion*) will be positive when \hat{n} is directed toward the center of the curvature. Thus, R>0 for counterclockwise flow and R<0 for clockwise flow. For the schematic given in Figure 4.11 we see that $\delta s=R\delta \psi$ and, by similarity, $\delta \hat{t}=\left|\hat{t}\right|\delta \psi$. Equating the expressions for $\delta \psi$ from both expressions we get

$$\delta\psi = \frac{\delta s}{R} = \frac{\delta \hat{t}}{|\hat{t}|} = \delta \hat{t} \tag{4.32}$$

since \hat{t} is a unit vector. Notice that as $\delta s \to 0$, $\delta \hat{t}$ is parallel to \hat{n} so that

$$\lim_{\delta s \to 0} \frac{\delta \hat{t}}{\delta s} = \frac{d\hat{t}}{ds} = \left(\frac{1}{R}\right) \hat{n} = \frac{\hat{n}}{R}.$$
 (4.33a)

Therefore,

$$\frac{d\hat{t}}{dt} = \frac{d\hat{t}}{ds}\frac{ds}{dt} = \left(\frac{\hat{n}}{R}\right)V = \left(\frac{V}{R}\right)\hat{n} \tag{4.33b}$$

since V = ds/dt by definition. Thus, we can rewrite (4.31) as

$$\frac{d\vec{V}}{dt} = \frac{dV}{dt}\hat{t} + \frac{V^2}{R}\hat{n} \tag{4.34}$$

which demonstrates that the acceleration following the motion is the sum of (1) the rate of change of the speed of the air parcel, and (2) its centripetal acceleration arising from curvature in the flow.

Since the Coriolis force acts normal to the flow it must be in the \hat{n} direction. In the northern hemisphere, the Coriolis force acts to the right of the motion, so in

the $-\hat{n}$ direction. Thus, we represent the Coriolis force as $COR = -(fV)\hat{n}$. In the southern hemisphere, the Coriolis force acts to the left of the motion, the \hat{n} direction. Given that latitude is positive (negative) in the northern (southern) hemisphere, by convention, the same expression for the Coriolis force

$$-f\hat{k} \times \vec{V} = -(fV)\hat{n} \tag{4.35}$$

is applicable in the southern hemisphere. The pressure gradient force has components in both the along-flow (\hat{t}) and across-flow (\hat{n}) directions so it can be rewritten as

$$-\nabla_p \phi = -\left(\frac{\partial \phi}{\partial s}\hat{t} + \frac{\partial \phi}{\partial n}\hat{n}\right). \tag{4.36}$$

Thus, the frictionless equation of motion (4.31) can be rewritten in natural coordinates as

$$\left(\frac{dV}{dt}\hat{t} + \frac{V^2}{R}\hat{n}\right) = -\left(\frac{\partial\phi}{\partial s}\hat{t} + \frac{\partial\phi}{\partial n}\hat{n}\right) - (fV)\hat{n} \tag{4.37}$$

which can be split into its along-flow component

$$\frac{dV}{dt} = -\frac{\partial \phi}{\partial s} \tag{4.38a}$$

and its across-flow component;

$$\frac{V^2}{R} + fV = -\frac{\partial \phi}{\partial n}.$$
 (4.38b)

For motion parallel to geopotential height contours, $\partial \phi/\partial s = 0$ (i.e. there is no change in ϕ in the along-flow direction), and the *speed* of the flow is constant. In this case, the flow can be classified into a number of simple categories based upon the relative contributions of the three terms in (4.38b), the \hat{n} -component equation of motion.

4.4.1 Geostrophic flow

Recall that in considering the \hat{n} equation of motion we are implicitly considering a flow in which the speed is constant. If we further consider a perfectly straight flow, then $|R| = \infty$. In such a case, only the Coriolis and pressure gradient forces remain from (4.38b) so that

$$fV = -\frac{\partial \phi}{\partial n}.\tag{4.39a}$$

Accordingly, the flow is in geostrophic balance and the geostrophic wind is expressed as

$$V_{g} = -\frac{1}{f} \frac{\partial \phi}{\partial n}.$$
 (4.39b)